PCCP

Cite this: *Phys. Chem. Chem. Phys.*, 2011, **13**, 14775–14783

www.rsc.org/pccp

PAPER

Why BLUF photoreceptors with roseoflavin cofactors lose their biological functionality†

Thomas Merz, Keyarash Sadeghian‡ and Martin Schütz*

Received 2nd May 2011, Accepted 16th June 2011
DOI: 10.1039/c1cp21386e

The photophysics of roseoflavin in three different environments is investigated by using *ab initio* and quantum mechanics/molecular mechanics methods. Intramolecular charge transfer is shown to be responsible for the quenching of the fluorescence in the gas phase, and in the water environment. However, for the roseoflavin incorporated into the blue light using flavin (BLUF) protein environment (substituting the native flavin) no such deactivation is found. The conical intersection between the locally excited state of the chromophore and the charge transfer state involving the tyrosine residue, which in the native BLUF domain is responsible for initiating the photocycle, is missing for the roseoflavin substituted protein. This explains the experimental observations of the lack of any photocycle, and the loss of the biological function of the BLUF photoreceptor reported earlier.

1 Introduction

Bacteria, plants and mammals use biological photoreceptors to perceive light from different parts of the visible spectrum. This allows them to regulate vital processes such as growth, development, color vision, circadian rhythms, and photomovement.[1] Depending on the embedded photo active chromophore or the initial steps involved in their photo-activation, the photoreceptors can be divided into six different families.[2] These families are the rhodopsins,[3] phytochromes,[4] xanthopsins,[5] phototropins,[6,7] cryptochromes[8] and BLUF (blue light using flavin adenine dinucleotide FAD) proteins.[9] The latter group, with a modified chromophore, is the subject of this paper.

Since the first discovered BLUF-domain containing flavoprotein, AppA from Rhodobacter sphaeroides,[10] several BLUF signaling domains have been found in prokaryotic and eukaryotic microorganisms. These include AppA,[11–16] BlrB,[17,18] Slr1694[19–23] and Tll0078.[24–26] Most of them have different physiological functions but share a common feature, namely the change in their UV/Vis-, as well as in their IR-spectra upon signaling state formation. It is therefore widely accepted that different BLUF domains should have the same or a similar mechanism for signaling state formation. The lack of unique crystal structures for both the dark- and light-adapted forms of BLUF-domains however has made the search for a conclusive mechanism of signaling state formation a challenge. A lot of proposals for this were made so far. Many different mechanisms were postulated,[27–32] which all have in common the very first step, *i.e.*, an electron transfer process from the nearby tyrosine residue to the flavin chromophore, thereby explaining the observed fluorescence quenching of the latter. Sadeghian *et al.* presented a plausible mechanism for the formation of the signaling state based on a systematic investigation of the potential energy surface.[33,34] There is strong evidence that after photo-excitation of the locally excited (LE) state of flavin, the tyrosine → flavin charge transfer (CT) state is populated *via* a conical intersection. This conical intersection seam has been investigated recently in detail by Udvarhelyi and Domratcheva.[35] At the level of the complete active space self-consistent field (CASSCF) method the authors located the minimum energy point on the seam along the relevant proton transfer reaction coordinate. Moreover, they also calculated pathways for the entire photo reaction leading to the final signaling state structure. The steps of this reaction cascade include tautomerization of the highly conserved glutamine residue and are in principle in agreement with the ones postulated by Sadeghian *et al.*[33,34]

Further attempts for a better understanding of the photo-activation of flavin containing BLUF and LOV domains include modification of the flavin chromophore. In this respect Mathes *et al.*[36] replaced the FAD chromophore of the wild type Slr1694 BLUF domain with roseoflavin (RoF, shown in Fig. 1). Zirak *et al.*[37] have investigated the photo-dynamics of the cofactor-exchanged Slr1694 (RoSlr) under both dark and light conditions. The behavior of riboflavin and RoF in different aqueous and organic solvents was also investigated for comparison.[37,38] The main observation from these experiments

Institute of Physical and Theoretical Chemistry, University of Regensburg, Universitätsstraße 31, D-93040 Regensburg, Germany. E-mail: martin.schuetz@chemie.uni-regensburg.de

† Electronic supplementary information (ESI) available. See DOI: 10.1039/c1cp21386e

‡ Present address: Chair of Theoretical Chemistry, Department of Chemistry, University of Munich (LMU), Butenandtstraße 7, D-81377 Munich, Germany.

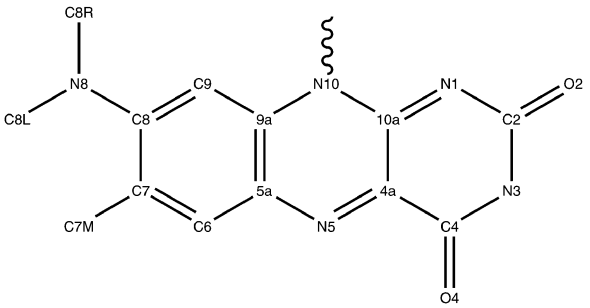

Fig. 1 Structure of roseoflavin (RoF). The main distinction between RoF and flavin is the dimethylamino (DMA) group. The dihedral angles τ and τ' defined as dihedral (C7, C8, N8, C8L) and dihedral (C7, C8, N8, C8R), respectively, are used often in text and therefore defined here.

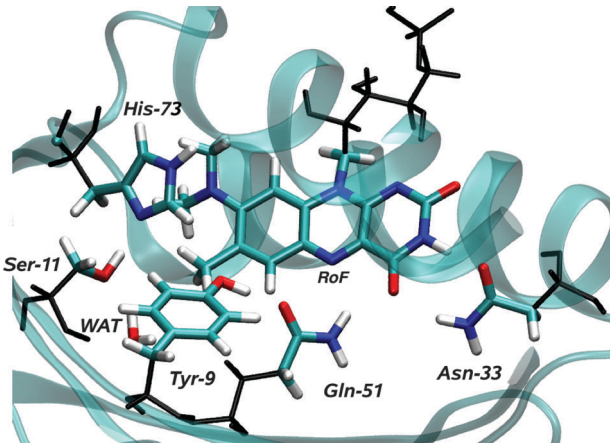

Fig. 2 QM region of RoF in protein.

is the lack of the photocycle, and with that the loss of the biological function of the protein by the flavin → RoF exchange.[37]

In this contribution the reason behind this loss of the biological function of the protein is investigated by using quantum mechanics/molecular mechanics (QM/MM) techniques. Furthermore, the electronic ground and excited states of RoF in water and in the gas phase are studied.

2 Computational details

2.1 RoF in the gas phase

For these pure QM calculations, density functional theory (DFT, with the BHLYP[39] functional) on the one hand, and CC2[40,41] on the other hand, were employed for geometry optimizations in the electronic ground state. The resulting BHLYP and CC2 optimized structures turn out to be very similar (RMSD: 0.05 a.u.). Geometry optimizations in the electronically excited states were carried out by using the time-dependent DFT (TD-DFT, BHLYP) and TD-CC2 response methods. As for the electronic ground state the optimized TD-DFT structure of the first excited state is very similar to that obtained at the level of CC2 response (RMSD: 0.09 a.u.).

2.2 RoF in water

The RoF moiety was solvated in a pre-equilibrated water droplet of 25 Å diameter containing 2142 water molecules. The boundary of 2.5 Å thickness was restrained by a quartic force of 24 kcal mol^{-1} $Å^{-2}$ using the miscellaneous mean-field potential (MMFP) implemented in CHARMM.[42] The main purpose of this part of our study is to include the influence of the water molecules, which are represented by "partial" charges in the one-electron part of the QM-Hamiltonian, on the photophysics of the RoF moiety. An extensive MD simulation was not carried out. An MM-minimized solvated structure was used as the starting point for the QM/MM geometry optimization. The QM region was restricted to the RoF moiety in these calculations. The same QM/MM settings were employed as for the calculations of RoF embedded in BlrB (*vide infra*). The potential parameters for the RoF chromophore were taken as identical to those employed for the flavin chromophore previously.[33] Still missing parameters were adopted from the CHARMM27 force field parameters for nucleic and amino acids.[43,44] For the complete list of potential parameters used in the present work see ESI†, Table S1–S3 and Fig. S1).

2.3 RoF in protein

In analogy to previous work[33] a monomer of the crystal structure of the FAD bound BLUF-domain protein (BlrB, PDB code: 1BYC)[18] was used in this study. The flavin moiety was replaced by the RoF by manually exchanging the methyl group at the C8 position (see Fig. 1) with the dimethylamino group. A pre-equilibrated water droplet with radius 20 Å containing 5187 water molecules was used to solvate the modified BLUF domain. Starting from the solvated minimized structure the same procedure as in the previous study[33] was used to obtain an MD trajectory. For two representative snap shots initial geometry optimizations at the force field level were carried out, followed by further optimizations at the QM/MM level. Only one of these was then taken for further investigations (*vide infra*).

For the QM/MM geometry optimizations, a QM region quite similar to that employed in previous work[33] was chosen (*cf.* Fig. 2). It includes the RoF moiety (electron acceptor), consisting of the 8-dimethyl-isoalloxazine with an additional methyl group at the N10 position, the Tyr-9 residue (electron donor), the Gln-51, and His-73 residues (the latter protonated at the nitrogen position denoted as NE in the crystal structure),[18] the water molecule WAT, as well as the Ser-11, and Asn-33 residues, which are in direct contact with the RoF chromophore. The ChemShell interface[45] was used for all QM/MM calculations. The QM/MM coupling was calculated using the charge shift scheme and link atoms. The MM part of the QM calculations was treated by the DL-POLY molecular dynamics package[46] with CHARMM force field parameters. The HDLCopt-optimizer,[47] implemented in ChemShell, was used for geometry optimizations. The Turbomole package[48] was utilized for the QM part. Here, DFT (employing the BP functional[49]) was used for the QM/MM geometry optimization of the electronic ground state. In the following, acronyms of the form DFT/Charmm are used to specify the individual

QM/MM methods, such as the combination of the DFT QM method with the Charmm forcefield.

Geometry optimizations of electronically excited states were performed with TD-DFT/Charmm (BHLYP functional). Furthermore to check on erroneous behavior of TD-DFT (particularly in the context of charge transfer states), single point vertical excitation energies at the optimized structures were also calculated at the level of TD-CC2/Charmm.

2.4 Basis sets

For the DFT calculations the def-SVP basis set[50] was employed. This basis set was also used for the CC2 and TD-CC2 geometry optimizations on the ground and excited state surfaces, respectively. Additionally, TD-CC2 single point vertical excitation energies were calculated in the aug-cc-pVDZ basis.[51] For the case of RoF embedded in the BLUF protein environment, the geometry optimizations at the TD-DFT level were carried out using the def-TZVP basis set.[52]

3 Results and discussion

3.1 RoF in the gas phase

Firstly, the question of the orientation of the DMA group relative to the ring system was studied. For this purpose a relaxed energy path along the dihedral angle τ (*cf.* Fig. 1) was calculated, which is depicted in Fig. 3.

Evidently, the DMA group is not in plane with the ring system at the minimum, but tilted by $\tau \approx \pm 60^{\circ}$. Vertical excitation energies at the minimum structure were calculated with TD-DFT- (BP, B3LYP, and BHLYP functionals), as well as TD-CC2-response. The electronic density difference plots for the excited states of interest, together with a schematic view of the energetics of these states, are all shown in Fig. 4.

As is evident from Fig. 4(d), the TD-DFT and TD-CC2 response methods predict different energetic orders for the π–π^* and n–π^* excitations. With the exception of the BP functional (shown here for comparison only), the π_1–π^* state is predicted as the lowest state. The energetic order and position of the π_2–π^* and n–π^* states differ from one method to another. Both of these states have significant charge transfer character (as is evident from the dipole moment changes relative to the ground state given in Fig. 4b and c) for which TD-DFT with local or semi-local functionals is bound to fail due to the inherent self-interaction error.[53]

The π_1–π^* (LUMO ← HOMO) state is the lowest excited state (S_1-state) with sizable oscillator strength and therefore easily populated by photo-excitation. For this state a geometry optimization at the TD-CC2 level was carried out. At the

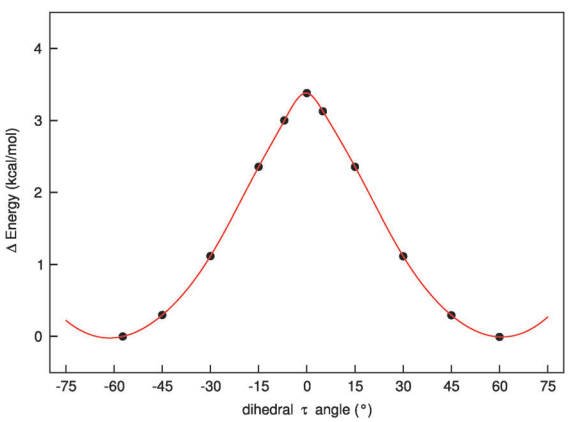

Fig. 3 RoF in the gas phase: relaxed energy path along the dihedral coordinate τ at the level of DFT (BHLYP functional).

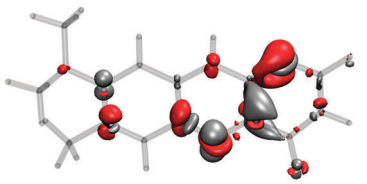

(a) S_1; $\pi_1 - \pi^*$; ω=2.51 eV; f=0.36; $\Delta\mu$=1.55 D

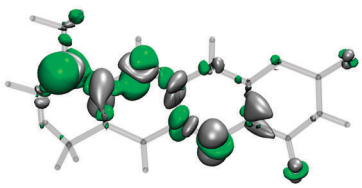

(b) S_2; $\pi_2 - \pi^*$; ω=3.22 eV; f=0.20; $\Delta\mu$=8.67 D

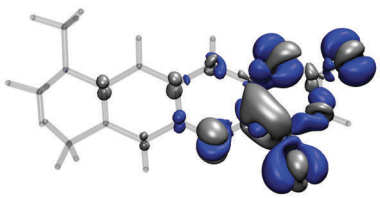

(c) S_3; $n \rightarrow \pi^*$; ω=3.36 eV; f=0.00; $\Delta\mu$=-6.38 D

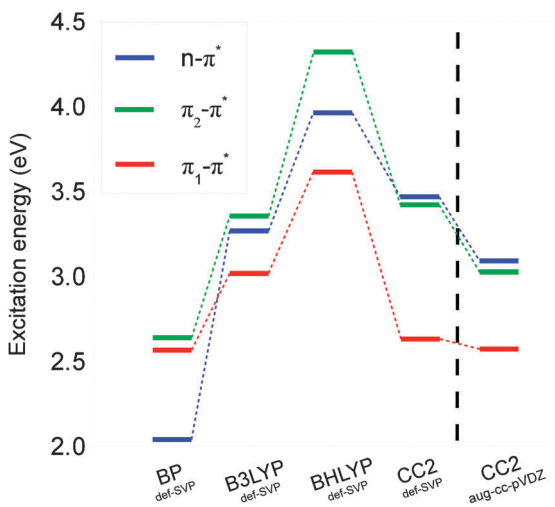

(d) Excitation energies in (eV)

Fig. 4 (a)–(c) TD-CC2 density differences (with respect to the ground state, aug-cc-pVDZ basis) of the n → π^*, π_1–π^*, and π_2–π^* excited states. The blue, red, and green isosurfaces at −0.004 show the regions with loss, the gray ones at +0.004 the regions with gain of electron density upon photo-excitation. The corresponding oscillator strengths f (on length representation) and the change of the dipole moment $\Delta\mu$ are denoted as well. (d) Vertical excitation energies of RoF in the gas phase calculated with TD-DFT and TD-CC2 response, respectively.

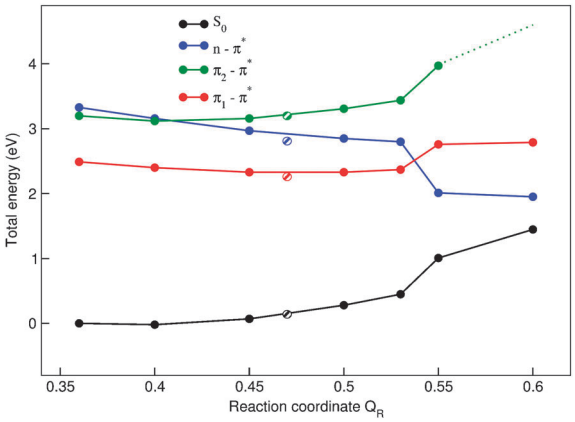

Fig. 5 Energies (in eV) of the relevant excited states relative to the ground state minimum energy at the relaxed structures along Q_R. The restrained geometry optimizations were performed with TD-CC2 response in the def-SVP basis on the energy surface of the lowest state, *i.e.*, on the π_1–π^* surface before, and on the n–π^* surface after the conical intersection. The plotted energies correspond to TD-CC2 response single point calculations at these relaxed structures in the bigger aug-cc-pVDZ basis. The point at $Q_R = 0.36$ corresponds to the FC point. The shaded points denote the S_1-minimum (at $Q_R = 0.47$).

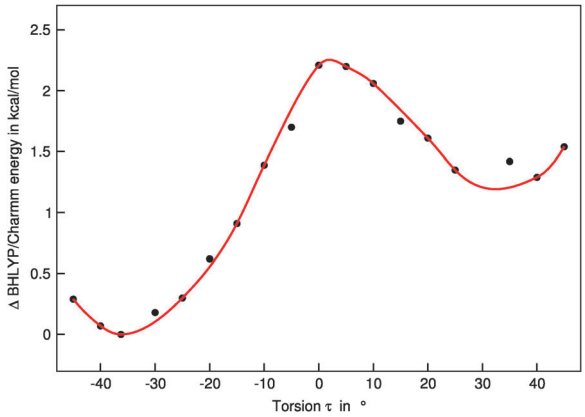

Fig. 6 BHLYP/Charmm energies of RoF in water along the dihedral angle τ (defined in Fig. 1).

resulting, fully relaxed geometry the $S_0 \rightarrow S_1$ transition maintains its π–π^* character. In contrast, the second and third excited states, *i.e.*, the π_2–π^* and the n–π^* states, switch their energetic order. At the Franck–Condon (FC) point the energy difference between the π_1–π^* and n–π^* state is about 0.85 eV. It drops down to 0.52 eV at the π_1–π^*-minimum structure (depicted as a red-dotted point in Fig. 5). Comparing the π_1–π^*-minimum and FC geometries reveals that the major changes occur only within some particular bond distances of the ring system of RoF. The DMA group, on other hand, remains in the same orientation and is therefore not affected by this relaxation process. In order to investigate this issue more thoroughly, an appropriate linear combination of these bond distances (see Fig. S2 and Table S4 in ESI† for the exact definition) was chosen as the coordinate Q_R. Along this coordinate, a relaxed energy path on the surface of the lowest state was calculated at the TD-CC2 level, starting from the FC point. This relaxed energy path is displayed in Fig. 5.

Evidently, the trace along Q_R leads to a conical intersection (CI) between the π_1–π^* and the n–π^* state. The step in the energies after the conical intersection is due to the sudden change in geometry, since the restrained geometry optimizations refer to the lowest state, which abruptly changes character at the CI. Continuing further along Q_R, but now on the energetically lower n–π^* state surface a second CI with the ground state then is encountered. We conclude that there is a fast deactivation channel from the photo-excited π_1–π^* state to the ground state *via* two CIs.

3.2 RoF in water

Also RoF in water, which represents one of the polar solvents employed in the experimental study by Zirak *et al.*,[38] was investigated by means of QM/MM. As for the gas phase, a relaxed energy path on the ground state along the dihedral angle τ was calculated, which is shown in Fig. 6. Evidently, the geometry with the DMA group in plane with the ring system does not correspond to a stable conformation and two minima at $\tau \approx \pm 35^\circ$ exist instead. The asymmetry of the QM/MM energy with respect to τ is due to the fact that the solvent environment is not fully relaxed at the $\tau = +35^\circ$ minimum conformation (no new MD optimization was carried out for $\tau \neq -35^\circ$). A symmetric potential energy surface with respect to the dihedral angle τ would be obtained once the water environment is fully adapted to the restrained RoF residue. This can be achieved, for example, by performing extensive QM/MM MD simulations for each dihedral restraint and averaging over all snap shots obtained as a result. However, for the purpose of this study we are only interested in the question about the DMA orientation and the results displayed in Fig. 6 clearly show that the planar ($\tau = 0^\circ$) structure is not stable. To explore the photophysics of RoF in water the QM/MM minimized structure with $\tau = -35^\circ$ ($\tau' = 156^\circ$) was further studied.

The vertical excitation energies of the two lowest excited states, calculated with TD-CC2/Charmm at the BHLYP/Charmm minimum structure above, are compiled in Fig. 7(c), the related density difference plots are given in Fig. 7(a) and (b). Comparison with Fig. 4(b) reveals that the S_1-state corresponds to the π_2–π^* charge transfer state in the gas phase which now is stabilized by the polar water environment. The calculated vertical excitation energy is in fortuitously good agreement with the maximum of the corresponding measured absorption band,[38] *i.e.*, 2.49 *vs.* 2.46 eV. The S_2 π_3–π^* state corresponds to yet another, higher lying state in the gas phase, and is irrelevant for the deactivation of photo-excited RoF in water (*vide infra*).

Attempts were made to find the minimum on the S_1 state surface. A preliminary restraint-free geometry optimization at the TD-CC2/Charmm level (data not presented) leads to two interesting observations. Firstly, the main degree of freedom involved in the relaxation on the S_1 surface is the rotation of the DMA group with respect to the ring system of the RoF moiety. Secondly, there is a large decrease in the S_1–S_0 energy gap along such a rotation, leading to a CI with the ground state for $\tau = -\tau' = 90^\circ$, where the response theory breaks down due to the degeneracy of the reference wave function. We conjecture that relaxation along this very coordinate is responsible for the deactivation of the first excited state.

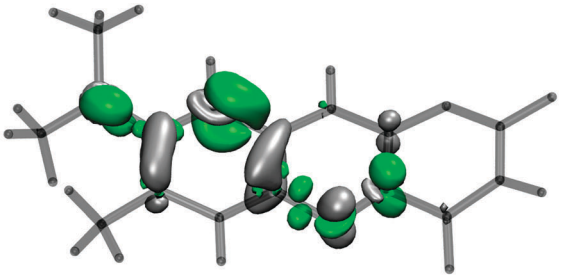

(a) S_1; $\pi_2 - \pi^*$; ω=2.49 eV (ω_{exp}=2.46 eV[38]); f=0.61; $\Delta\mu$=1.73 D

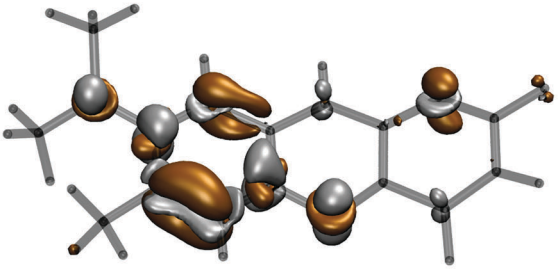

(b) S_2; $\pi_3 - \pi^*$; ω=3.08 eV; f=0.13; $\Delta\mu$=0.00 D

State	gas phase analogy	S_0-minimum ω	S_0-minimum f	$S_1^{\Delta Q=0.5}$ ω	$S_1^{\Delta Q=0.5}$ f
S_1	$\pi_2 - \pi^*$	2.49	0.613	0.31	0.091
S_2	$\pi_3 - \pi^*$	3.08	0.132	2.20	0.016

(c)

Fig. 7 TD-CC2/Charmm (aug-cc-pVDZ basis) electron density difference plots for (a) the S_1 or π_2–π^* state, (b) the S_2 or the π_3–π^* state. Gray and green/brown areas show the regions with gain and loss of electron density relative to the ground state, respectively. The isosurfaces correspond to values of ±0.004. (c) Corresponding vertical excitation energies, ω (in eV), and oscillator strengths, f (in length representation), calculated at the S_0-minimum and $S_1^{\Delta Q\,=\,0.5}$ structure.

A relaxed energy path along τ on the excited state surface was computed to examine this hypothesis more carefully. We decided to take a different reaction coordinate to impose the desired τ and τ' values. It turned out that taking the dihedral angles directly leads to an unbalanced path with metastable restrained geometries, caused by the out of plane angle of the DMA group. Instead a bond difference coordinate, defined as $\Delta Q = d$(C8R–C7M) − d(C8L–C7M) (atom labels are taken from Fig. 1) was employed. Calculating the relaxed energy path along ΔQ avoids this problem. The resulting curve calculated with TD-CC2/Charmm is depicted in Fig. 8; the dihedral angles τ and τ' corresponding to a certain ΔQ value are also given. Evidently, rotation of the DMA group rapidly leads downhill from the FC point on the S_1 surface towards a CI with the ground state, which is encountered for a perpendicular orientation of the DMA group with $\tau = -\tau' = 90°$. The rotation of the DMA group thus represents a fast deactivation channel for the S_1 state of RoF solvated in water.

3.3 RoF in BlrB

Since the true crystal structure of the BlrB BLUF domain with flavin being replaced by RoF is not available the QM/MM structure of previous work[33] (which is based on the crystal structure of Schlichting and co-workers, PDB code: 1BYC)[18] was altered by replacing the methyl group at the C8 position of the cofactor by the dimethylamino (DMA) group. To adapt this new RoF chromophore to the adjacent residues within the flavin binding pocket of the BlrB BLUF domain a 500 ps molecular dynamics simulation was carried out, prior to selecting relevant structures for the subsequent QM/MM calculations. Since the initial structure was already equilibrated previously the adaptation of RoF and the adjacent residues is the prime concern here. To monitor this adaptation the root mean square deviation (RMSD) values of the positions of the atoms of the relevant residues in the vicinity of the RoF moiety, *i.e.*, those in H-bonding and/or van der Waals contact with RoF, were recorded during the MD simulation. The result is plotted in ESI†, Fig. S4a. It can be seen that the RMSD values fluctuate between 0.5 and 0.8 Å, which is indicating (i) that the RoF moiety has adapted itself to its new environment, and (ii) that there is enough space for the larger RoF in the binding pocket. The fluctuations in the RMSD values can be traced back mainly to the water (WAT) molecule, which exhibits different orientations relative to the Tyr-9 moiety. A similar observation was already made previously in ref. 33 for the wild type structure, where the WAT molecule can act as a H-donor to either the hydroxy group, or the aromatic ring of the Tyr-9 residue. As in the previous study, a conformation was chosen with the WAT molecule acting as H-donor to the ring of Tyr-9.

One of the key questions regarding the electronic structure of RoF in the BLUF protein is whether the DMA group (for definition see Fig. 1) takes a planar orientation towards the ring system of the RoF moiety or not. The structure is considered as *planar*, if $\tau \approx 0°$ and $\tau' \approx 180°$, otherwise as *non-planar*. Measuring these two dihedrals along the obtained trajectory may lead to the conclusion that the DMA group remains more or less planar (see Fig. S4b in ESI†, where the measured values for τ and τ' are plotted). As is evident from this figure the two dihedral angles fluctuate around –10° and 170° respectively. However, the force field parameters used for RoF (see Table S3 in ESI†) are designed only for a planar orientation of the DMA group with respect to the RoF ring system, hence for a more reliable answer an unbiased QM/MM investigation is required. Considering the stability of the residues within the RoF binding pocket in the production run within the last 100 ps (*cf.* Fig. S4 in ESI†) one representative snap shot (at 420 ps) from the MD trajectory was chosen for the further QM/MM investigations. This snap shot then was further optimized using the DFT/Charmm (BP functional) method, which leads to a non-planar orientation of the DMA group ($\tau = -40°$ and $\tau' = +160°$). The geometry so obtained, denoted for further reference as $RoF_p^{(np)}$, is depicted in Fig. 9(a).

In order to avoid any bias arising from the choice of the initial geometry a further QM/MM geometry optimization was performed with the DMA group first restrained to a planar orientation (by setting τ and τ' to 0 and 180°, respectively) and fully relaxed thereafter in a second step. The resulting geometry (with $\tau = -170°$ and $\tau' = 2°$), denoted in the following as $RoF_p^{(pl)}$, is shown in Fig. 9(b).

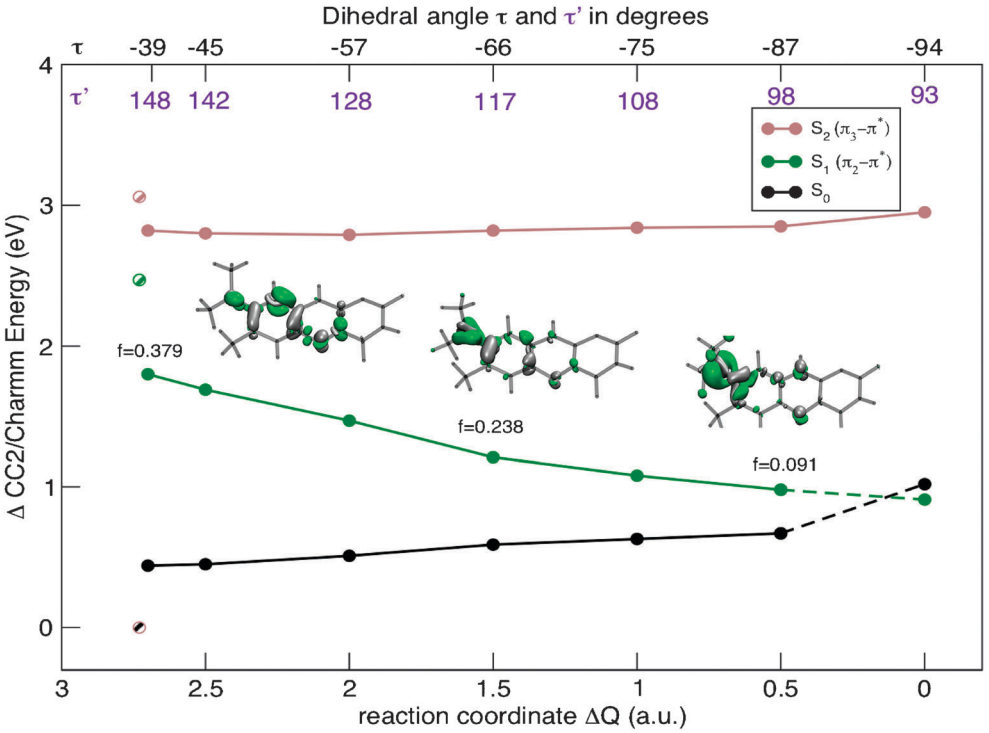

Fig. 8 TD-CC2/Charmm energy (in eV) of the ground (S_0) and S_1 state plotted along the path obtained *via* constrained geometry optimization on the S_1 state. The dihedral angles τ and τ' for all, the oscillator strength (f) and the density difference for some restrained optimized geometries are also shown. The shaded points correspond to the FC geometry.

The $RoF_p^{(pl)}$ structure is energetically more stable (by about 4 kcal mol^{-1}) than the *non-planar* $RoF_p^{(np)}$ conformer. Single point MP2/Charmm calculations (employing the aug-cc-pVDZ basis set) carried out for both structures confirm the BP/Charmm result. Here, the planar $RoF_p^{(pl)}$ structure is about 3 kcal mol^{-1} more stable than its non-planar $RoF_p^{(np)}$ counterpart.

The planarity of the DMA group of RoF is expected to be influenced by the protonation state and orientation of the adjacent residues. Here, we have identified two possible conformations of the RoF cofactor within the binding pocket of the BlrB BLUF domain. A definite answer to the question of DMA orientation with respect to the ring system requires further experimental information about the structure and protonation of the amino acids in the close neighborhood of the RoF chromophore. In the following, based on these two stable conformations $RoF_p^{(pl)}$ and $RoF_p^{(np)}$ at hand, the excited states relevant for the photocycle of the wild-type BLUF domains are explored, *i.e.*, the locally excited (LE) state (localized on the chromophore), and the charge transfer (CT) state shifting electron density from the tyrosine residue to the chromophore. The vertical excitation energies for these two states at the $RoF_p^{(pl)}$ and $RoF_p^{(np)}$ geometries, calculated with TD-DFT/Charmm (BHLYP, def-TZVP basis), and TD-CC2/Charmm (aug-cc-pVDZ basis, *cf.* Section 2) are shown schematically in Fig. 10. The corresponding electron density difference plots (relative to the ground state density), calculated with TD-CC2/Charmm (cc-pVDZ basis), are given in Fig. 11.

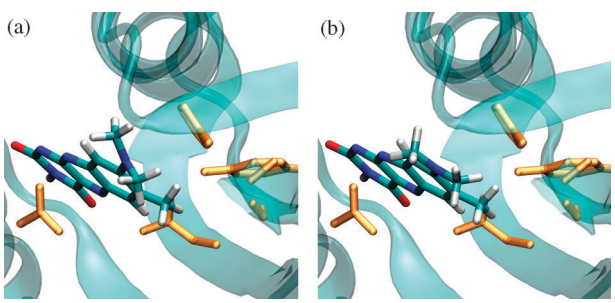

Fig. 9 BP/Charmm optimized structures of RoF in the BlrB flavin binding pocket where the non-planar $RoF_p^{(np)}$ (a) and planar $RoF_p^{(pl)}$ (b) conformations are shown.

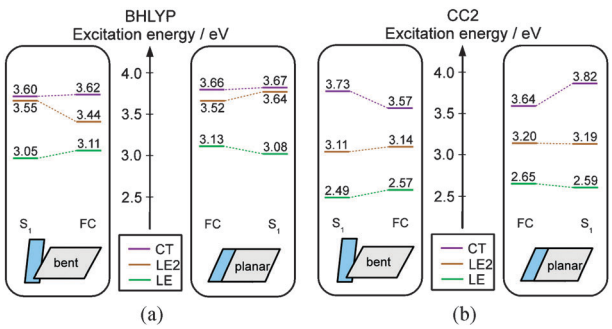

Fig. 10 QM/MM excitation energies of the planar and non-planar RoF conformations at the Franck–Condon (FC) point, and at the S_1 (LE) optimized structures, calculated (a) with TD-DFT/Charmm (BHLYP) in the def-TZVP basis, and (b) with TD-CC2/Charmm in the aug-cc-pVDZ basis.

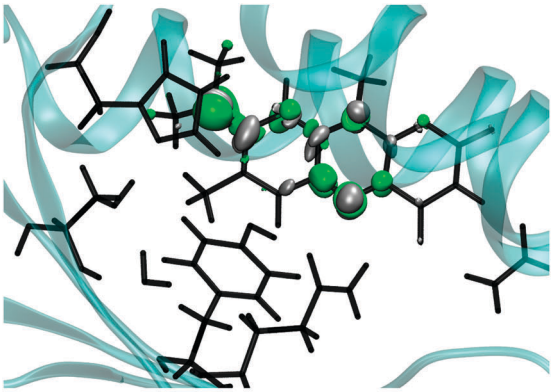

(a) S_1; LE; ω=2.57 eV (ω_{exp}=2.38 eV[37]); f=0.67; $\Delta\mu$=3.71 D

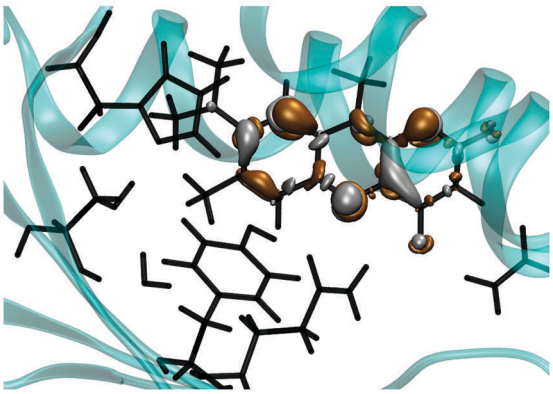

(b) S_2; LE2; ω=3.14 eV; f=0.03; $\Delta\mu$=1.66 D

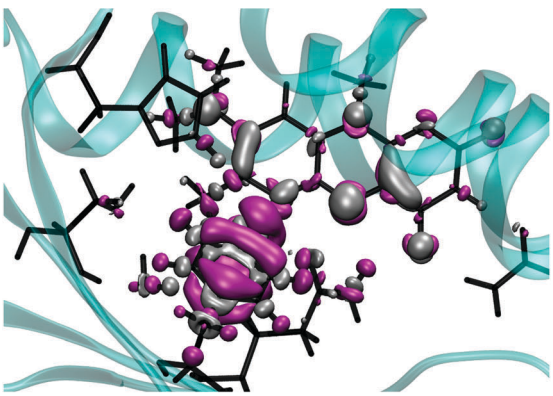

(c) S_3; CT; ω=3.57 eV; f=0.00; $\Delta\mu$=18.70 D

Fig. 11 TD-CC2/Charmm (with cc-pVDZ basis) electron density difference plots for (a) the LE, (b) the LE2 and (c) the CT state at the $RoF_p^{(np)}$ geometry. Gray and green/brown/purple areas show the regions with gain and loss of electron density relative to the ground state, respectively. The isosurfaces correspond to values of ±0.003. The corresponding oscillator strengths f (length representation, calculated with aug-cc-pVDZ basis) and the change of the dipole moment $\Delta\mu$ are given as well.

The LE state with its high oscillator strength (f = 0.6–0.7 for the planar and non-planar RoF conformations) is the state initially populated by the photo-excitation. It is a π–π^* excitation as in the native BLUF with a flavin cofactor, yet comparison of the two density difference plots, *i.e.*, Fig. 11(a) of the present paper with Fig. 6a of ref. 33, reveals some differences. For example, in the 4a–10a C–C bond (*cf.* Fig. 1) density *decreases* in RoF while it *increases* in native flavin BLUF. Consequently, the RoF 4a–10a bond distance *increases* significantly (by about 5 pm) on relaxation from the FC point to the LE minimum, while the native flavin 4a–10a bond distance *decreases* towards the LE minimum.

The calculated vertical excitation energy of the RoF LE state is somewhat larger than the measured value (2.57 *vs.* 2.38 eV[37]), but still well within the expected error bars of the method.

In order to initiate a photocycle similar to that observed in the native BLUF domains, population transfer from the LE state to the tyrosine → RoF CT state *via* a CI then has to take place. TD-DFT is known to underestimate long range charge transfer states. Here, this underestimation is alleviated by employing the BHLYP functional containing 50% exact HF-exchange. In fact, in the planar, as well as in the non-planar structure the CT state lies energetically above the LE state, which is in agreement with the TD-CC2/Charmm results. However, TD-DFT/Charmm (BHLYP) overestimates the excitation energies of the LE states in comparison to TD-CC2/Charmm. The TD-CC2/Charmm excitation energies themselves are rather stable with respect to the basis set size and do not show any dramatic changes when the basis set is augmented by diffuse functions (*cf.* Table S5 in ESI†). The excitation energy of the LE state is rather insensitive with respect to the orientation of the DMA group and remains at about 2.6 eV for both the planar and the non-planar conformations. In contrast to the native BLUF domain the tyrosine → RoF CT state at about 3.6 eV, which is relevant for the biological functionality of the protein, corresponds not to the second, but to the third excited state. Between the LE state and the latter there is another locally (on the RoF subunit) excited state with very low oscillator strength, denoted in the following as LE2. LE and LE2 appear to correspond to the S_1 and S_2 states of RoF in water, respectively, as can be seen by comparing the electron density difference plots of Fig. 11 and 7.

Starting from the FC points QM/MM geometry optimizations were carried out with TD-DFT/Charmm (BHLYP, def-TZVP basis) on the LE state surfaces of both conformations. Subsequently, vertical excitation energies at the respective LE-minimum structures were calculated with TD-CC2/Charmm in the aug-cc-pVDZ basis. The resulting excitation energies at the respective LE minimum structures are also shown in Fig. 10. Evidently, for both the planar and non-planar RoF conformations the CT state not only remains above the LE state, but the LE–CT gap even *increases* on going from the FC points to the LE minima. The LE2 state in between, on the other hand, hardly changes. In particular, no crossing of states is observed. This implies that there exists no conical intersection close to the LE minimum for RoF substituted BLUF domains, and the tyrosine → RoF CT state thus *cannot* be populated efficiently after photo-excitation. This is in strong contrast to the case of native BLUF domains, where the LE–CT gap closes towards the LE-minimum,[33–35] and explains the experimental observations as the lack of a photocycle and the loss of the biological function of RoF substituted BLUF domains.[37]

4 Conclusions

Based on the results obtained in this study, the photophysics of RoF in the gas phase, in water, and embedded in the BlrB BLUF domain, are shown schematically in Fig. 12. Even though the individual conical intersections were not mapped out in detail here the following hypotheses can be put up.

In the gas phase, the bright locally excited π_1–π^* state is deactivated *via* a CI with the dark n–π^* state. The latter is deactivated further *via* a second CI with the ground state. In water, on the other hand, the initially populated state is deactivated directly *via* a CI with the ground state. The n–π^* state does not seem to play a role there. Of further interest are the modes which are mainly responsible for deactivating the excited states. In vacuum, an in-plane ring mode appears to be driving the deactivation process, which would fit to the picture of a planar intramolecular charge transfer (PICT)[54] model.

In water, on the other hand, the rotation of the DMA group with respect to the ring system is of prime importance for deactivation, which in turn would fit to the picture of a twisted intramolecular charge transfer (TICT)[55] model. Actually, the significant fluorescence quenching of RoF in water observed by Zirak *et al.*[37,38] was also assigned to a TICT model (on the basis of low temperature measurements) by these authors.

The situation is quite different for RoF embedded in the BlrB BLUF domain. In the TD-CC2/Charmm calculations performed in this work the n–π^* state does not exist among the six lowest states. Instead, the locally excited (LE) state of RoF, and the tyrosine → RoF charge transfer (CT) state do occur, which are already known from previous work on the native BlrB BLUF domain. A QM/MM geometry optimization of the LE state however shows that in strong contrast to the native BLUF domain no low lying conical intersection near the LE minimum exists, which would be instrumental for population transfer from the LE to the CT state. The CT state thus is not populated after photo-excitation, and, as a consequence, the whole reaction cascade leading *via* proton transfer and tautomerization of the glutamine residue to the signaling state in the native BLUF case cannot take place. This explains the experimental observations such as the absence of a photocycle, and the loss of the biological functionality of RoF substituted BLUF domains. Thus, in contrast to the conjecture made in the conclusions of ref. 37 a TICT deactivation of RoF is not the prime reason for their dysfunctionality. However, calculations with an artificially increased τ angle of the DMA group of RoF in the protein environment indicate that a TICT mechanism analogous to that of RoF in water may be responsible for the fluorescence quenching of RoF in the BLUF domain (see Fig. S5 in ESI†).

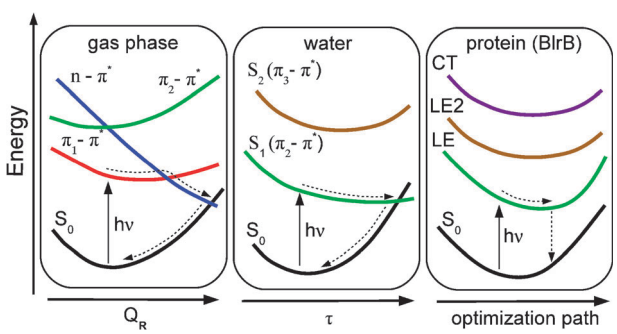

Fig. 12 Qualitative picture of the different excited state characteristics of RoF in different environments. In the gas phase a quasi-PICT mechanism *via* intramolecular charge-shifting, whereas in water a quasi-TICT mechanism *via* a intramolecular charge-shifting between the π-system and the DMA-group is observed. In the BLUF protein environment no CI between the CT- and LE-state is found in contrast to the wild type domain.

Acknowledgements

The authors thank Dr Marco Bocola for useful discussions. This project is part of the Graduate College Chemical Photocatalysis (GRK 1626) in Regensburg, funded by the Deutsche Forschungsgemeinschaft.

References

1 J. M. Christie and W. R. Briggs, *J. Biol. Chem.*, 2001, **276**, 11457–11460.
2 M. A. van der Horst and K. J. Hellingwerf, *Acc. Chem. Res.*, 2004, **37**, 13–20.
3 W. D. Hoff, K. H. Jung and J. L. Spudlich, *Annu. Rev. Biophys. Biomol. Struct.*, 1997, **26**, 223.
4 P. H. Quail, *Philos. Trans. R. Soc. London, Ser. B*, 1998, **353**, 1399.
5 R. Kort, W. D. Hoff, M. van West, A. R. Kroon, S. M. Hoffer, K. H. Vlieg, W. Crielaand, J. J. V. Beeumen and K. J. Hellingwerf, *EMBO J.*, 1996, **15**, 3209.
6 E. Huala, P. W. Oeller, E. Liscum, I. S. Han, E. Larsen and W. R. Briggs, *Science*, 1997, **278**, 2120.
7 T. E. Swartz, S. B. Corchnoy, J. M. Christie, J. W. Lewis, I. Szundi, W. R. Briggs and R. A. Bogomolni, *J. Biol. Chem.*, 2001, **276**, 36493.
8 M. Ahmad and A. R. Cashmore, *Nature*, 1993, **366**, 162–166.
9 M. Gomelsky and G. Klug, *Trends Biochem. Sci.*, 2002, **27**, 497–500.
10 S. Masuda and C. Bauer, *Cell (Cambridge, Mass.)*, 2002, **110**, 613.
11 W. Laan, M. van der Horst, I. van Stokkum and K. Hellingwerf, *Photochem. Photobiol.*, 2003, **78**, 290.
12 V. Dragnea, M. Waegele, S. Balascuta, C. Bauer and B. Dragnea, *Biochemistry*, 2005, **44**, 15978.
13 S. Masuda, Y. Tomida, H. Ohta and K.-I. Takamiya, *J. Mol. Biol.*, 2007, **368**, 1223.
14 P. Zirak, A. Penzkofer, T. Schiereis, P. Hegemann, A. Jung and I. Schlichting, *Chem. Phys.*, 2005, **315**, 142.
15 M. Gauden, I. H. M. van Stokkum, J. M. Key, D. C. Lührs, R. van Grondelle, P. Hegemann and J. T. M. Kennis, *Proc. Natl. Acad. Sci. U. S. A.*, 2006, **103**, 10895.
16 A. Jung, J. Reinstein, T. Domratcheva, R. L. Shoeman and I. Schlichting, *J. Mol. Biol.*, 2006, **362**, 717.
17 P. Zirak, A. Penzkofer, T. Schiereis, P. Hegemann, A. Jung and I. Schlichting, *J. Photochem. Photobiol., B*, 2006, **83**, 180.
18 A. Jung, T. Domratcheva, M. Tarutina, Q. Wu, W.-H. Ko, R. Shoeman, M. Gomelsky, K. H. Gardner and I. Schlichting, *Proc. Natl. Acad. Sci. U. S. A.*, 2005, **102**, 12350.
19 K. Hasegawa, S. Masuda and T.-A. Ono, *Biochemistry*, 2004, **43**, 14979.
20 S. Masuda, K. Hasegawa, A. Ishii and T.-A. Ono, *Biochemistry*, 2004, **43**, 5304.
21 K. Hasegawa, S. Masuda and T.-A. Ono, *Plant Cell Physiol.*, 2005, **46**, 136.
22 P. Zirak, A. Penzkofer, C. Lehmpfuhl, T. Mathes and P. Hegemann, *J. Photochem. Photobiol., B*, 2007, **86**, 22.
23 H. Yuan, S. Anderson, S. Masuda, V. Dragnea, K. Moffat and C. Bauer, *Biochemistry*, 2006, **45**, 12687.
24 Y. Fukushima, K. Okajima, Y. Shibata, M. Ikeuchi and S. Itoh, *Biochemistry*, 2005, **44**, 5149.

25 K. Okajima, Y. Fukushima, H. Suzuki, A. Kita, Y. Ochiai, M. Katayama, Y. Shibata, K. Miki, T. Noguchi, S. Itoh and M. Ikeuchi, *J. Mol. Biol.*, 2006, **363**, 10.
26 A. Kita, K. Okajima, Y. Morioto, M. Ikeuchi and K. Miki, *J. Mol. Biol.*, 2005, **349**, 1.
27 W. Laan, M. Gauden, S. Yeremenko, R. van Grondelle, J. T. M. Kennis and K. J. Hellingwerf, *Biochemistry*, 2006, **45**, 51–60.
28 M. Gauden, I. H. M. van Stokkum, J. M. Key, D. C. Luhrs, R. van Grondelle, P. Hegemann and J. T. M. Kennis, *Proc. Natl. Acad. Sci. U. S. A.*, 2006, **103**, 10895–10900.
29 M. Gauden, J. S. Grinstead, W. Laan, I. H. M. van Stokkum, M. Avila-Perez, K. C. Toh, R. Boelens, R. Kaptein, R. van Grondelle, K. J. Hellingwerf and J. T. M. Kennis, *Biochemistry*, 2007, **46**, 7405.
30 A. L. Stelling, K. L. Ronayne, J. Nappa, P. J. Tonge and S. R. Meech, *J. Am. Chem. Soc.*, 2007, **129**, 15556–15564.
31 T. Domratcheva, B. L. Grigorenko, I. Schlichting and A. V. Nemukhin, *Biophys. J.*, 2008, **94**, 3872–3879.
32 J. Götze and P. Saalfrank, *J. Photochem. Photobiol., B*, 2009, **94**, 87–95.
33 K. Sadeghian, M. Bocola and M. Schütz, *J. Am. Chem. Soc.*, 2008, **130**, 12501.
34 K. Sadeghian, M. Bocola and M. Schütz, *Phys. Chem. Chem. Phys.*, 2010, **12**, 8840–8846.
35 A. Udvarhelyi and T. Domratcheva, *Photochem. Photobiol.*, 2010, **87**, 554–563.
36 T. Mathes, C. Vogl, J. Stolz and P. Hegemann, *J. Mol. Biol.*, 2009, **385**, 1511–1518.
37 P. Zirak, A. Penzkofer, T. Mathes and P. Hegemann, *J. Photochem. Photobiol., B*, 2009, **97**, 61.
38 P. Zirak, A. Penzkofer, T. Mathes and P. Hegeman, *Chem. Phys.*, 2009, **358**, 111.
39 A. D. Becke, *J. Chem. Phys.*, 1993, **98**, 1372–1377.
40 O. Christiansen, H. Koch and P. Jørgensen, *Chem. Phys. Lett.*, 1995, **243**, 409–418.
41 C. Hättig and F. Weigend, *J. Chem. Phys.*, 2000, **113**, 5154–5161.
42 B. R. Brooks, R. E. Bruccoleri, B. D. Olafson, D. J. States, S. Swaminathan and M. Karplus, *J. Comput. Chem.*, 1983, **4**, 187.
43 A. D. MacKerell, D. Bashford, M. Bellott, R. L. Dunbrack, J. D. Evanseck, M. J. Field, S. Fischer, J. Gao, H. Guo, S. Ha, D. Joseph-McCarthy, L. Kuchnir, K. Kuczera, F. T. K. Lau, C. Mattos, S. Michnick, T. Ngo, D. T. Nguyen, B. Prodhom, W. E. Reiher, B. Roux, M. Schlenkrich, J. C. Smith, R. Stote, J. Straub, M. Watanabe, J. Wiorkiewicz-Kuczera, D. Yin and M. Karplus, *J. Phys. Chem. B*, 1998, **102**, 3586–3616.
44 N. Foloppe and A. D. MacKerell, *J. Comput. Chem.*, 2000, **21**, 86.
45 P. Sherwood, A. H. de Vries, M. F. Guest, G. Schreckenbach, C. R. A. Catlow, S. A. French, A. A. Sokol, S. T. Bromley, W. Thiel, A. J. Turner, S. Billeter, F. Terstegen, S. Thiel, J. Kendrick, S. C. Rogers, J. Casci, M. Watson, F. King, E. Karlsen, M. Sjøvoll, A. Fahmi, A. Schäfer and C. Lennartz, *THEOCHEM*, 2003, **1**, 632.
46 W. Smith, C. W. Yong and P. M. Rodger, *Mol. Simul.*, 2002, **28**, 385–471.
47 S. R. Billeter, A. J. Turner and W. Thiel, *Phys. Chem. Chem. Phys.*, 2000, **2**, 2177–2186.
48 R. Ahlrichs, M. Bär, M. Häser, H. Horn and C. Kölmel, *Chem. Phys. Lett.*, 1989, **162**, 165.
49 A. D. Becke, *Phys. Rev. A: At., Mol., Opt. Phys.*, 1988, **38**, 3098–3100.
50 A. Schäfer, H. Horn and R. Ahlrichs, *J. Chem. Phys.*, 1992, **97**, 2571.
51 D. E. Woon and T. H. Dunning, Jr., *J. Chem. Phys.*, 1993, **98**, 1358–1371.
52 A. Schäfer, C. Huber and R. Ahlrichs, *J. Chem. Phys.*, 1994, **100**, 5829.
53 A. Dreuw, J. L. Weisman and M. Head-Gordon, *J. Chem. Phys.*, 2003, **119**, 2943.
54 T. Yoshihara, S. Druzhinin and K. Zachariasse, *J. Am. Chem. Soc.*, 2004, **126**, 8535.
55 Z. R. Grabowski, K. Rotkiewicz and W. Rettig, *Chem. Rev.*, 2003, **103**, 3899.